Modelling and control of particulate systems - three industrial(ly based) case studies

Denis Dochain, Céline Casenave, C. Henri, L. Noon

Available online at www.sciencedirect.com

ScienceDirect

IFAC PapersOnline CONFERENCE PAPER ARCHIVE

IFAC PapersOnLine 53-2 (2020) 11404–11409

Modelling and control of particulate systems - three industrial(ly based) case studies

D. Dochain * **C. Casenave** ** **C. Henri** * **L. Noon** *

* *ICTEAM, Université Catholique de Louvain, Louvain-la-Neuve Belgium (e-mail: denis.dochain@uclouvain.be)*

** *MISTEA, Universit Montpellier, INRAE, Institut Agro, Montpellier, France (e-mail: fceline.casenave@supagro.inra.fr)*

Abstract: This paper deals with the modelling and control application for three case studies of particulate systems: one agglomeration process (for anti-foam agents in washing machine soap), and two crystallization processes, one related to one ice-cream crystallization, the other related to the pharmaceutical industry.

Keywords: Particulate systems, population balance model, partial differential equations, adaptive linearizing control.

1. INTRODUCTION

Particulate systems play an increasing role in industrial applications, and the particulate size distribution is indeed more and more important when dealing with product quality. More specifically, in many industrial applications, a key issue is to guarantee that the size distribution remains close enough to a specific reference value, i.e centred on a reference mean value with a variance as small as possible, or to correspond to a specific size distribution. As a matter of example, in the case of ice cream, it is well known that the quality, that is the hardness and the texture of the ice cream, depends on the ice crystal size distribution (CSD). For example, depending on the mean crystal size, or more precisely on the dispersion of crystal sizes (that is on the shape of the CSD), the obtained texture of the ice cream is more or less grainy. Some physical properties of the ice cream, as for example its viscosity, also depend on the CSD (Casenave et al. (2014), Casenave et al. (2013), Casenave et al. (2012)). In the context of the production of granulated additive particles (in the mentioned example of the production of anti-foam agents, for instance), it is essential to produce particles whose size remains close to that of the detergent powder so that the solid mixture remains as homogeneous as possible to make sure that both can dissolve at the same time (Henri et al. (2006a), Henri et al. (2006b)).

2. POPULATION BALANCE MODELS

The dynamics of particulate systems are basically described by partial integro-differential equations, i.e. partial differential equations (PDE's) that contain an integral term. These belong to the category of population balance models (Ramkrishna (2000)).

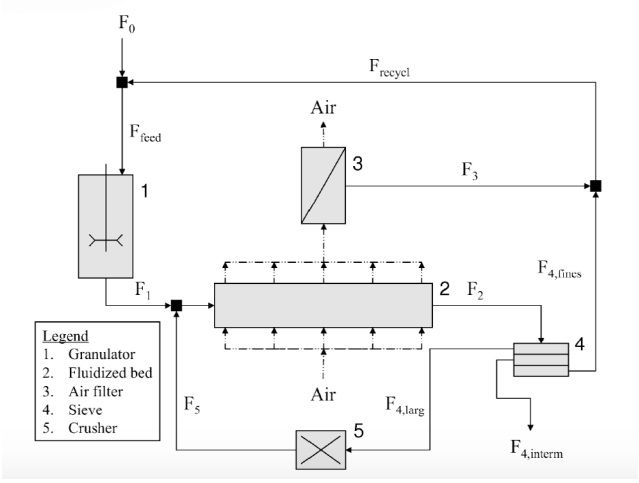

Fig. 1. Flow sheet of the production process of granulated particles

2.1 The agglomeration process

As a matter of illustration, let us first consider the production of granulated particles mentioned above. The (industrial) process is indeed composed of a (high-shear) granulator and a fluidised bed reactor (see Figure 1). The fine fresh powder inflow rate (F_0) and a binder liquid enter the granulator in which particles agglomerate. The particle outflow rate (F_1) goes through the fluidised bed reactor where it is dried and undergoes a second agglomeration. In the fluidised bed reactor, the finer particles are removed by a vertical air flow. The air and these particles are then separated in a filter. The particle flow rate (F_3) is recycled at the top of the process. The fluidized bed particle outflow rate (F_2) is divided in three flow rates into a sieve:

$$F_2 = F_{4,fines} + F_{4,larg} + F_{4,interm} \quad (1)$$

where $F_{4,fines}$, $F_{4,larg}$ and $F_{4,interm}$ represent the flow rates of the finer particles that are recycled at the top

10.1016/j.ifacol.2020.12.575

of the process, of the larger particles that are crushed and recycled to the fluidised bed reactor, and of the intermediate particles that are the desired product, respectively.

Let us assume that there is no germination, growth or breakage, and that both the granulator and the fluidised bed reactor are operated in perfectly mixed conditions with a constant reacting medium volume. We obtain the following population balance equation from mass balance on the number of particles $n(v,t)$ of size volume v in the granulator (index 1) and in the fluidised bed reactor (index 2)(Henri et al. (2006b)):

$$\begin{aligned}\frac{\partial n_1(v,t)}{\partial t} &= \frac{1}{2}\int_0^v \beta_1(t,u,v-u)n_1(u,t)n_1(v-u,t)du \\ &\quad - \int_0^\infty \beta_1(t,u,v)n_1(u,t)n_1(v,t)du + F_0(v,t) \\ &\quad + F_3(v,t) + F_{4,fines}(v,t) - F_1(v,t) \qquad (2)\\ \frac{\partial n_2(v,t)}{\partial t} &= \frac{1}{2}\int_0^v \beta_2(t,u,v-u)n_2(u,t)n_2(v-u,t)du \\ &\quad - \int_0^\infty \beta_2(t,u,v)n_2(u,t)n_2(v,t)du \\ &\quad + F_1(v,t) + F_5(v,t) - F_3(v,t) - F_2(v,t) \qquad (3)\end{aligned}$$

with

$$F_1(v,t) = \frac{q_1 n_1(v,t)}{V_1},\ F_2(v,t) = \frac{q_2 n_2(v,t)}{V_2} \qquad (4)$$

$$F_{4,fines}(v,t) = \begin{cases} F_2(v,t) & \text{if } v < v_{sieve,fines} \\ 0 & \text{if } v \geq v_{sieve,fines} \end{cases} \qquad (5)$$

$$F_{4,larg}(v,t) = \begin{cases} F_2(v,t) & \text{if } v \geq v_{sieve,larg} \\ 0 & \text{if } v < v_{sieve,larg} \end{cases} \qquad (6)$$

$$F_3(v,t) = \begin{cases} F_1(v,t) + F_5(v,t) & \text{if } v < v_{sieve,fines} \\ 0 & \text{if } v \geq v_{sieve,fines} \end{cases} \qquad (7)$$

In the above equations, q_1, q_2, V_1, V_2, $\beta_1(t,u,v)$, $\beta_2(t,u,v)$ are the volumetric outflow rates, the volumes and the coalescence kernels in the granulator and in the fluidised bed reactor, respectively. The first two terms on the right-hand side of both equations (2)(3) are the birth and death rates of agglomerates resulting from agglomeration, respectively.

Equation (7) assumes that the fines are instantaneously removed from the fluidised bed reactor. The fines particles have a size-volume v such that $v < v_{bed,fines}$.

2.2 The crystallization process

As a second example, let us consider the crystallization of ice cream. A schematic view of the pilot crystallizer is shown on Figure 2 (Casenave et al. (2014)). The pilot plant is located at IRSTEA Antony (France). The ice cream crystallizer is a 0.40 meter long cylindric scraped surface heat exchanger, with inner diameter of 0.05 meter. The mix sorbet, which is mainly composed of sugar, gum and water, is first put in a mix storage tank which is refrigerated at a temperature T_0 of $5°C$. The mix sorbet is then fed to the crystallizer by a piston pump. Within the vessel jacket of the crystallizer, a refrigerant fluid, whose temperature T_e is called the evaporation temperature, is continuously vaporizing to cool down the mix sorbet. When the temperature of the mix sorbet goes below the saturation temperature T_sat, the crystallization occurs. Some ice crystals appear on the inner wall of the cylinder and are scraped by two scraper blades which turn with a rotation speed N_scrap and therefore mix the ice.

The dynamics of the ice cream crystallization are deduced from mass and energy balance equations. The mass balance results in a population balance model for the number $n(L,t)$ of crystals per cubic meter of length L. The mass balance considers transport, crystal growth, nucleation and breakage, while the radial diffusion is assumed to be negligible. If the plug flow reactor is approximated, from an input-output point of view, by a Continuous Stirred-Tank Reactor (CSTR) with a transport delay [1] (to account for the fluid transport in the freezer), then we get the following equation :

$$\frac{\partial n}{\partial t} = -Dn - \frac{\partial (Gn)}{\partial L} + N\delta_{(L-L_\mathrm{c})} + B_\mathrm{b} \qquad (8)$$

where δ denotes the Dirac function. D is the dilution rate, i.e. the ratio of the mass flow rate m_{fr} over the product of the density of the solution ρ_s and the volume $V$of the freezer ($D = \frac{m_{fr}}{\rho_s V}$). L and L_c are the crystal length variable and the initial crystal length, and G, N, B_b are the growth rate, nucleation rate, and net increase of crystals number by breakage, respectively.

The growth and nucleation rates are expressed by [2] :

$$G = \beta(T_\mathrm{sat} - T),\ \text{and}\ N = \alpha S\left(T_\mathrm{sat} - T_e\right)^2, \qquad (9)$$

where T_sat is the saturation temperature, and α, β are some kinetic parameters.
Because of the scraper, the crystals can also be broken. We assume that a particle of size L' is broken into two particles of the same length L. The volume of ice is considered unchanged by the fragmentation and a spherical shape is assumed. Under these assumptions, the net increase of particles by breakage B_b, can be expressed as [3] :

$$B_\mathrm{b} = \epsilon N_\mathrm{scrap}\,\phi_\mathrm{i}^\nu \left(2\,2^{2/3}\,L\Psi(\sqrt[3]{2}\,L) - L\Psi(L)\right), \qquad (10)$$

with N_scrap the dasher rotation speed, ϵ a breakage coefficient, ϕ_i the ice fraction and ν the breakage power coefficient which is taken equal to 0.

Under the same hypotheses, the energy balance equation is written as follows :

$$\frac{dU}{dt} = \underbrace{-D(U-U_0)}_{\text{transport}} + \underbrace{h_\mathrm{e}S(T_\mathrm{e}-T)}_{\text{wall heat transfer}} + \underbrace{\mu\dot{\gamma}^2}_{\text{viscous dissipation}} \qquad (11)$$

where U and T are the respective volumetric internal energy and temperature at the outlet of the freezer, U_0 is the internal energy at the inlet of the freezer, T_e is the evaporation temperature, h_e is the convective heat transfer coefficient and μ is the viscosity. The effective shear rate $\dot{\gamma}$ is expressed as $\dot{\gamma} = 2\pi\chi N_\mathrm{scrap}$ with χ the viscous

[1] The transport delay does not appear in the equation (8) and (11) because the input variables, that is the crystal size distribution and the temperature of the mix at the inlet of the freezer, are constant.
[2] Only heterogeneous nucleation at the freezer wall ($r = R_\mathrm{e}$) is considered here.
[3] Under these assumptions, the relation between L' and L is given by $L' = 2^{1/3}L$.

dissipation coefficient. The quantity $S = \frac{2R_e}{R_e^2 - R_i^2}$ is the ratio of the circumference over the surface of the section of the freezer, R_e and R_i denoting the maximum and minimum diameters of the cylindrical freezer, respectively.

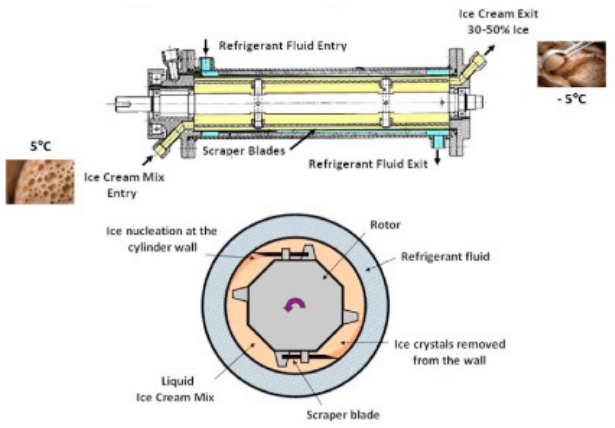

Fig. 2. Schematic view of the ice cream crystallizer

3. POPULATION MODEL VALIDATION

A key issue in population balance models is to select the appropriate functions that characterize the different mechanisms that are involved in the transformation of the size distribution of the particles. For the ice cream crystallization process, detailed information on the selection of the growth, nucleation and breakage terms can be in found in (Benkhelifa et al (2011)) and (Benkhelifa et al (2008)). For the agglomeration, the selection and the validation on industrial data of the agglomeration kernels $\beta_1(t,u,v)$ and $\beta_2(t,u,v)$ has been performed as follows.

The coalescence kernel $\beta_i(t,u,v)$ (i= 1,2) is often separated into a time-dependent rate-constant and a size-dependent kernel (Nilpawar et al. (2005) Biggs et al (2003)):

$$\beta_i(t,u,v) = \beta_{i,0}(t)\beta_i^*(u,v) \tag{12}$$

The size-dependent kernel $\beta_i^*(u,v)$ describes the aggregation rate as a function of the two colliding particles volumes.

In our study, the aggregation rate constants $\beta_{1,0}(t)$ and $\beta_{2,0}(t)$ have been considered as fitting parameters. The literature provides a wide range of size-dependent aggregation kernels : some of them are based on physical models, others are empirically-based. In our study, the use of four kernels has been investigated: the size-independent kernel (SIK), the equipartition of kinetic energy kernel (EKE), the equipartition of translational momentum kernel (ETM) and a square kernel (SQR):

$$\mathrm{S}IK : \beta_i^*(u,v) = 1 \tag{13}$$

$$\mathrm{E}KE : \beta_i^*(u,v) = (u+v)^2\sqrt{\left(\frac{1}{u^3}+\frac{1}{v^3}\right)} \tag{14}$$

$$\mathrm{E}TM : \beta_i^*(u,v) = (u+v)^2\sqrt{\left(\frac{1}{u^6}+\frac{1}{v^6}\right)} \tag{15}$$

$$\mathrm{S}QR : \beta_i^*(u,v) = \left(\frac{1}{u+v}\right)^2 \tag{16}$$

The SIK is chosen for its simplicity. It favours all interactions equally. This model is fully empirical and offers a good comparison with the three other kernels which are physically-based (Hounslow et al (2001)). The EKE kernel is presented by (Hounslow et al (2001)). In this model, it is assumed that collisions occur as a consequence of random motion. This kernel favours large-small particle interactions. In the ETM kernel, each granule is assumed to be subject to the same randomly fluctuating impulses (Hounslow (1998)). The last kernel favours small-small particle interactions.

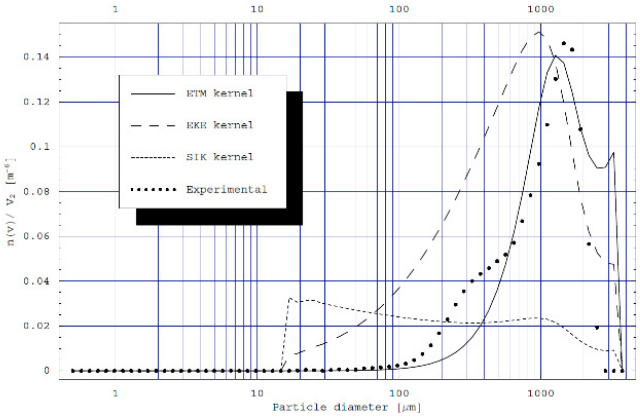

Fig. 3. Particle size distribution at the output of the fluidised bed reactor

As a matter of illustration and validation, the different distributions at the outlet of the fluidised bed reactor are shown in Figure 3, as compared to experimental distribution data. Figure 3 shows that the ETM kernel shape exhibits a better fit to the experimental distribution. With the EKE kernel a lot of particles remains in the range 100-1000 microns. The distribution obtained with the SIK kernel is not in good agreement with the experimental data.

4. REDUCED ORDER MODELS

The analysis of such models in the context of infinite dimensional systems is an increasingly active research area (e.g. Beniich et al. (2017)). Control design can be performed directly from the PDE model (this known as *early lumping* (Ray (1978)), see for example (Palis (2019)) or (Beniich et al. (2019)). Yet the PDE models are often discretized for control design (*late lumping*). One typical approach in particulate systems is to consider the moments of increasing order. The number of moments equations that are finally kept, and the closure of the truncated system are some important questions.

4.1 Ice cream crystallization

In the ice cream case study (Casenave et al. (2014)) for instance, the first four moment equations are independent of the higher order ones, and the energy balance equation only involves moments of order 3 or less, so that the considered reduced system finally reduced to a set of 5 ordinary differential equations (ODE's).

The method of moments consists in multiplying the population balance equation by L^j and then integrating it from

$L = 0$ to $L = \infty$. Applying the method of moments to our crystallization model, we get, for all $j \geq 0$:

$$\frac{dM_j}{dt} = -DM_j + j\,G\,M_{j-1} + N\,L_{\mathrm{c}}^j + B\left(2^{1-\frac{j}{3}} - 1\right) M_{j+1} \tag{17}$$

where the j^{th} order moment M_j is given by :

$$M_j(t) = \int_0^\infty L^j \Psi(L,t) dL \tag{18}$$

and

$$B = \epsilon N_{\mathrm{scrap}}. \tag{19}$$

with $\Psi(L,t)$ the crystal size distribution and L the crystal length.

The saturation temperature is supposed to depend only on M_3, that is $T_{\mathrm{sat}} = T_{\mathrm{sat}}(M_3)$. As a consequence, G and N can be expressed as functions of the variables M_3 and T, and M_3 and T_{e} respectively (i.e. $G = G(M_3, T)$ and $N = N(M_3, T_{\mathrm{e}})$).

Moreover, if we consider the ice crystals as spherical particles (as in Benkhelifa et al (2011)), then we have:

$$\phi_{\mathrm{i}} = \frac{\pi}{6} M_3, \tag{20}$$

Since both the volume and the pressure are assumed to be constant, the internal energy U is equal to the enthalpy H which is indeed composed of two terms:

- the enthalpy related to the crystallization:
$$-\Delta H \rho_i \phi_i$$
where $-\Delta H$ ρ_i and ϕ_i are the specific fusion latent heat, the mass density of the ice, and the ice fraction, respectively;
- the enthalpy of the solute and of the water:
$$\rho_s\left(\omega_0 C_s + (1-\omega_0) C_w\right) T$$
where ρ_s, ω_0, C_s, C_w and T are the mass density of the solution, the initial mass fraction of solute (sucrose), the solute specific heat capacity, the water specific heat capacity, and the temperature, respectively.

This means that equation (11) can be rewritten with the temperature T as the state variable:

$$\begin{aligned}\frac{dT}{dt} &= D\left(T_0 - T\right) + K_2\left(T_{\mathrm{e}} - T\right) \\ &\quad + N_{\mathrm{scrap}}^2 K_3 \mu + K_1\left(3GM_2 + NL_{\mathrm{c}}^3\right)\end{aligned} \tag{21}$$

with the following quantities :

$$K_0 = \rho_s\left(\omega_0\, C_{\mathrm{s}} + (1-\omega_0) C_{\mathrm{w}}\right),\ T_0 = \frac{U_0}{K_0}, \tag{22}$$

$$K_1 = \frac{\pi}{6}\frac{\Delta H\, \rho_i}{K_0},\ K_2 = \frac{h_{\mathrm{e}} S}{K_0},\ K_3 = \frac{(2\pi\chi)^2}{K_0}. \tag{23}$$

Finally, if the viscosity μ is assumed to depend only on the third moment M_3, the temperature T, and the dasher rotation speed N_{scrap} (i.e. $\mu = \mu(M_3, T, N_{\mathrm{scrap}})$), then the system composed of the first four moment equations and the temperature equation is closed. In fact all the dynamical quantities of this system are functions of the moments M_0, M_1, M_2, M_3, the temperature T and the input variables T_{e}, D and N_{scrap}. The moment based reduced model reads then as follows :

$$\frac{dM_0}{dt} = -DM_0 + N + BM_1 \tag{24}$$

$$\frac{dM_1}{dt} = -DM_1 + GM_0 + NL_{\mathrm{c}} + c_1 BM_2 \tag{25}$$

$$\frac{dM_2}{dt} = -DM_2 + 2GM_1 + NL_{\mathrm{c}}^2 + c_2 BM_3 \tag{26}$$

$$\frac{dM_3}{dt} = -DM_3 + 3GM_2 + NL_{\mathrm{c}}^3 \tag{27}$$

$$\begin{aligned}\frac{dT}{dt} &= D\left(T_0 - T\right) + K_2\left(T_{\mathrm{e}} - T\right) \\ &\quad + N_{\mathrm{scrap}}^2 K_3 \mu + K_1\left(3GM_2 + NL_{\mathrm{c}}^3\right)\end{aligned} \tag{28}$$

with $\mu = \mu(M_3, T, N_{\mathrm{scrap}})$, $G = G(M_3, T)$, $N = N(M_3, T_{\mathrm{e}})$, $B = B(N_{\mathrm{scrap}})$ and the following constants :

$$c_1 = 2^{\frac{2}{3}} - 1,\ c_2 = 2^{\frac{1}{3}} - 1. \tag{29}$$

M_0, M_1, M_2 and M_3 represent the number of particles, the sum of characteristic lengths and the images of the total area and volume of the crystals per cubic meter at the outlet of the freezer respectively. Their respective units are $[\mathrm{m}^{-3}]$, $[\mathrm{m}^{-2}]$, $[\mathrm{m}^{-1}]$ and $[-]$.

A detailed identification procedure for the reduced model of the ice crystallization process can be found in (Casenave et al. (2014)).

4.2 Pharmaceutical crystallization proccess

In our study for the crystallization in the pharmaceutical industry, the context was the scaling up of the process. Our study (Noon (2007)) was based on experiments performed in batch reactors. For the low scale experiments, breakage phenomena can be neglected [4], and nucleation (germination) is explicitly included in the boundary conditions (since the reactor is seeded: this privileges what is known as the secondary germination (Mullin (2001))), i.e. for $L = 0$.

The population balance model reduces to:

$$\frac{\partial n}{\partial t} = -\frac{\partial (Gn)}{\partial L} \tag{30}$$

$$n(0,t) = \frac{N(t)}{G(t)} \tag{31}$$

where $N(t)$ is the nucleation (secondary germination) rate.

In line with experimental evidence, the growth rate $G(t)$ is assumed to be independent of the size of the crystals, and is a function of the solute concentration $C(t)$ and of its saturation concentration C_{sat}. Indeed crystallization is closely related to the notion phase change between liquid and solid, and that of the solubility which is the thermodynamic equilibrium parameter between liquid phase and solid phase. This phase equilibrium is usually represented by a concentration vs temperature curve (at constant pressure), as it is represented in Figure 4 (glycine-water). From such a curve, we can deduce a relation of the saturation concentration as a function of the temperature, $C_{sat}(T)$. It is known that crystallization can take place in a zone close

[4] for large scale operation, these are not negligible anymore and is clearly part of the upscaling study of the crystallization process, but this part of the study cannot be reported here.

to the solubility curve. This zone is called the metastable zone (in Figure 4, it is defined by the zone between the blue curve and the green curve). As a consequence, the growth rate $G(t)$ and the nucleation rate $N(t)$ are typically modelled as a function of the sursaturation ratio

$$S = \frac{C(t) - C_{sat}(T)}{C_{sat}(T)}$$

Moreover Arrhenius type dependence with respect to the temperature, $exp(-E/RT)$ (with E an activation energy and R the ideal gas constant) is considered, It is also known that the nucleation rate $N(t)$ depends on the third order moment M_3 (which represents the total volume of the crystals) (see Mullin (2001)). Therefore $G(t)$ and $N(t)$ can be modelled as follows:

$$G(t) = k_g e^{-\frac{E_g}{RT}} \left(\frac{C(t) - C_{sat}(T)}{C_{sat}(T)} \right)^g \tag{32}$$

$$N(t) = k_n e^{-\frac{E_n}{RT}} \left(\frac{C(t) - C_{sat}(T)}{C_{sat}(T)} \right)^n M_3 \tag{33}$$

where k_g and k_n are kinetic constants.

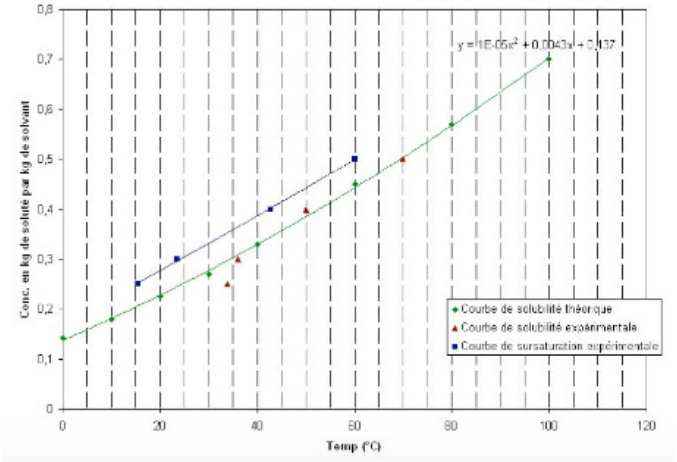

Fig. 4. Solubility curve and metastable zone

In the present instance, the population balance is completed by a mass balance equation for the solute concentration C and by an energy balance, and once we apply the methods of moments, we obtain the following set of ODE's for the whole system dynamics:

$$\frac{dM_0}{dt} = k_n e^{-\frac{E_n}{RT}} \left(\frac{C(t) - C_{sat}(T)}{C_{sat}(T)} \right)^n M_3 \tag{34}$$

$$\frac{dM_1}{dt} = k_g e^{-\frac{E_g}{RT}} \left(\frac{C(t) - C_{sat}(T)}{C_{sat}(T)} \right)^g M_0 \tag{35}$$

$$\frac{dM_2}{dt} = 2k_g e^{-\frac{E_g}{RT}} \left(\frac{C(t) - C_{sat}(T)}{C_{sat}(T)} \right)^g M_1 \tag{36}$$

$$\frac{dM_3}{dt} = 3k_g e^{-\frac{E_g}{RT}} \left(\frac{C(t) - C_{sat}(T)}{C_{sat}(T)} \right)^g M_2 \tag{37}$$

$$\frac{dC}{dt} = -3\rho k_v k_g e^{-\frac{E_g}{RT}} \left(\frac{C(t) - C_{sat}(T)}{C_{sat}(T)} \right)^g M_2 \tag{38}$$

$$\frac{dT}{dt} = -\frac{\Delta H}{C_p} 3\rho k_v k_g e^{-\frac{E_g}{RT}} \left(\frac{C(t) - C_{sat}(T)}{C_{sat}(T)} \right)^g M_2 + \frac{UA}{MC_p}(T_e - T) \tag{39}$$

where k_v, ΔH, C_p, U, A, M and T_e are a volumetric shape factor, the heat of reaction, the specific heat of the solute, the heat exchanger coefficient, the heat exchange surface, the mass of solute, and the heat exchanger temperature, respectively.

Parameter identification via a least square method has been performed for the above model (Noon (2007)).

5. CONTROL

For the above case study, a linear temperature profile (from 50°C to 31°C over a period of 30 hours) has been applied as a reference profile over the batch period by implementing a simple PI controller whose control input was the heat exchanger temperature T_e (see Figure 5). Such temperature guarantees that the process remains the metastable zone (see Figure 6).

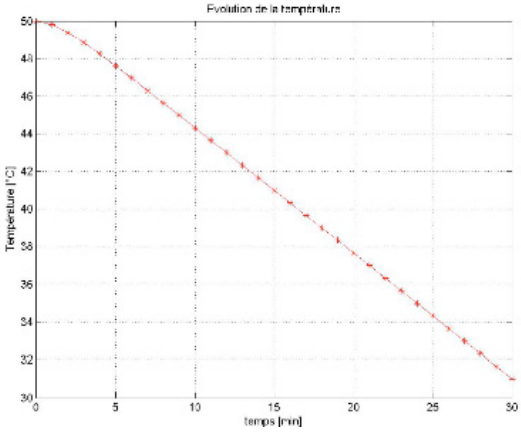

Fig. 5. Temperature profile in the batch reactor

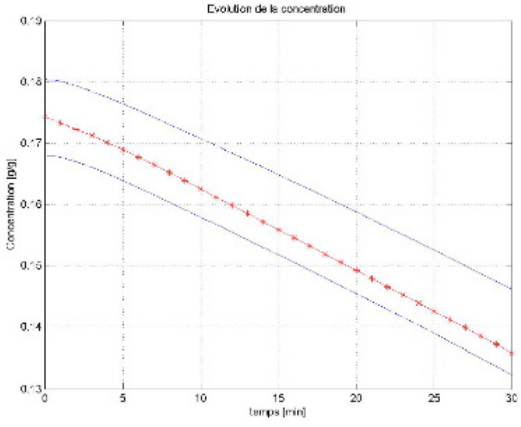

Fig. 6. Solute concentration in the batch reactor

A detailed control design has been performed also for the ice cream crystallization process (Casenave et al. (2013)). In the ice cream industry, the type of final desired product (large cartons (sqrounds) or ice creams on a stick) determine the viscosity at which the ice cream has to be produced. One of the objectives of the ice cream crystallization processes is therefore to produce an ice cream of specified viscosity. In practice this means that the objective is to control the viscosity μ of the product at the outlet of the freezer, or more precisely at the measurement

point, located a bit further than the outlet of the freezer. At this measurement point, the temperature of the ice cream is close to the saturation temperature $T_{sat}(M_3)$. In other words, the output variable to be controlled is $y = T_{sat}(M_3)$. A detailed study showed that the best control input will be the compressor rotation speed V_{comp}. In the present instance, it is more precisely a cascade control that has been considered with two control loops: a primary loop to control T_{sat} via the action of the heat exchanger temperature T_e, and a secondary loop to control T_e with V_{comp}. An adaptive linearizing controller has been designed on the basis of the moment model (24)-(28)(Casenave et al. (2013)). Figure 7 shows experimental results of the application of the cascade adaptive controller to the freezer.

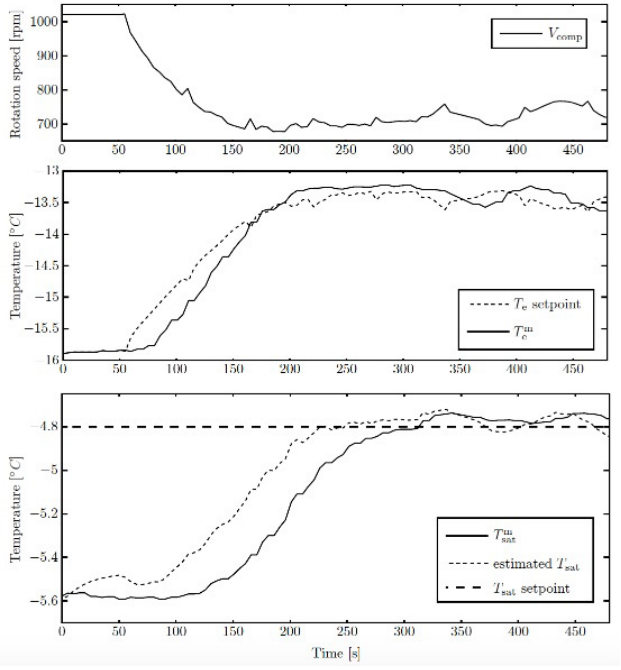

Fig. 7. Control of the ice cream crystallization: experimental results

6. CONCLUSIONS

In this paper we have reviewed three case studies of modelling and control of particulate systems with one industrial agglomeration process and two crystallization processes (one industrial pharmaceutical process, one pilot scale ice cream crystallization process). Note that our application studies have also been applied to other industrial particulate systems, like nanoparticles production.

REFERENCES

Beniich N., B. Abouzaid and D. Dochain (2019). Extremum seeking control for a mass structured cell population balance model in a bioreactor. submitted to *IFAC World Congress*, Berlin.

Beniich N., B. Abouzaid and D. Dochain (2017). On the existence and positivity of a mass structured cell population model. *Applied MathematicalScience*, 12(19):921-934.

Benkhelifa H. , M. Arellano, G. Alvarez, and D. Flick (2011). Ice crystals nucleation, growth and breakage modelling in a scraped surface heat exchange. *11th Internation Congress on Engineering and Food (ICEF)*, Athens, Greece, May 2011.

Benkhelifa H., A. H. Amamou, G. Alvarez, and D. Flick (2008). Modelling fluid flow, heat transfer and crystallization in a scraped surface heat exchanger. *Acta Horticulturae (ISHS)*, 802, 163-170.

Biggs C., C. Sanders, A. Scott, A. Willemse, A. Hoffman, T., Instone, A. Salman and M. Hounslow (2003). Coupling granule properties and granulation rates in high-shear granulation. *Powder Technology*, 130, 162-168.

Casenave C., D. Dochain, G. Alvarez, M. Arellano, H. Benkhelifa and D. Leducq (2014). Model identification and reduction for the control of an ice cream crystallization process. Chemical Engineering Science, 119, 274-287.

Casenave C., D. Dochain, G. Alvarez, M. Arellano, H. Benkhelifa and D. Leducq (2013). Control of a nonlinear ice cream crystallization process. IFAC Proceedings Volumes, 46(23), 717-722.

Casenave C., D. Dochain, G. Alvarez, H. Benkhelifa, D. Flick and D. Leducq (2012). Steady-state and stability analysis of a population balance based nonlinear ice cream crystallization model. Proc. ACC, 6461-6466.

Henri C., B. Haut, D. Dochain and V. Halloin (2006). Modeling of an industrial agglomeration process. *Proc. ISCRE 19*, Sept. 3-6, Posdam/Berlin, Germany, 869-870.

Henri C., B. Haut, D. Dochain and V. Halloin (2006). Modeling of an agglomeration process. *CESAME, Université catholique de Louvain*, intenal report, 14 pages.

Hounslow M., J. Pearson and T. Instone, T. (2001). Tracer studies of high-shear granulation : ii. population balance modeling. *AIChE Journal*, 47 (9), 1984-1999.

Hounslow M. (1998). The population balance as a tool for understanding particle rate processes. *Kona*, 16, 179-193.

Mullin J. (2001). *Crystallization*. Fourth ed., Elsevier, Butterworth-Heinemann, Amsterdam.

Nilpawar A., G. Reynolds, A. Salman and M. Hounslow (2005). Kinematics in high shear granulation. *Proceedings of the 8th International Symposium on Agglomeration*, 23-29.

Noon L. (2007). Modélisation et identification d'un modle de cristallisation de l'industrie pharmaceutique. *CESAME, Université catholique de Louvain*, intenal report, 40 pages.

Palis S. (2019). Adaptive discrepancy based control of continuous fluidized bed spray granulation with external sieve-mill cycle. *IFAC-PapersOnLine* , 52(2), 218-222.

Ramkrishna D. (2000). *Population Balances: Theory and Applications to Particulate Systems in Engineering*. Academic Press, London.

Ray W.H. (1978). Some recent applications of distributed parameter systems theory - A survey. *Automatica*, 14, 281-287.